



COLLEGE OF ENGINEERING
NUCLEAR ENGINEERING AND RADIOLOGICAL SCIENCES
UNIVERSITY OF MICHIGAN

Dynamic Tailoring of Intrinsic Nanoprecipitation Behavior in Steels via Additive Manufacturing

T.M. Kelsy Green^a, Niyanth Sridharan^b, Xiang Chen^c, Kevin G. Field^d

^a University of Michigan-Ann Arbor

^b Oak Ridge National Laboratory; Current: Lincoln Electric, India

^c Oak Ridge National Laboratory

^d Oak Ridge National Laboratory; Current: University of Michigan-Ann Arbor

T.M. Kelsy Green:
tmkgreen@umich.edu

Niyanth Sridharan:
Niyanth_Sridharan@LincolnElectric.in

Xiang Chen (Frank):
chenx2@ornl.gov

Kevin Field:
kgfield@umich.edu

Extreme Nuclear Environments

Advanced Reactor Design Considerations for Structural Materials

Temp. Range: 300-1,000°C

Damage Level: ≤ 200 dpa

Stress: ≤ 150 MPa

Corrosion

Advanced Reactor Radiation Effects

- Radiation hardening and embrittlement
- Phase instabilities
- Irradiation creep
- Swelling
- He embrittlement

Desired Material Features Achieved with Fine, stable precipitates

Good long-term thermal aging

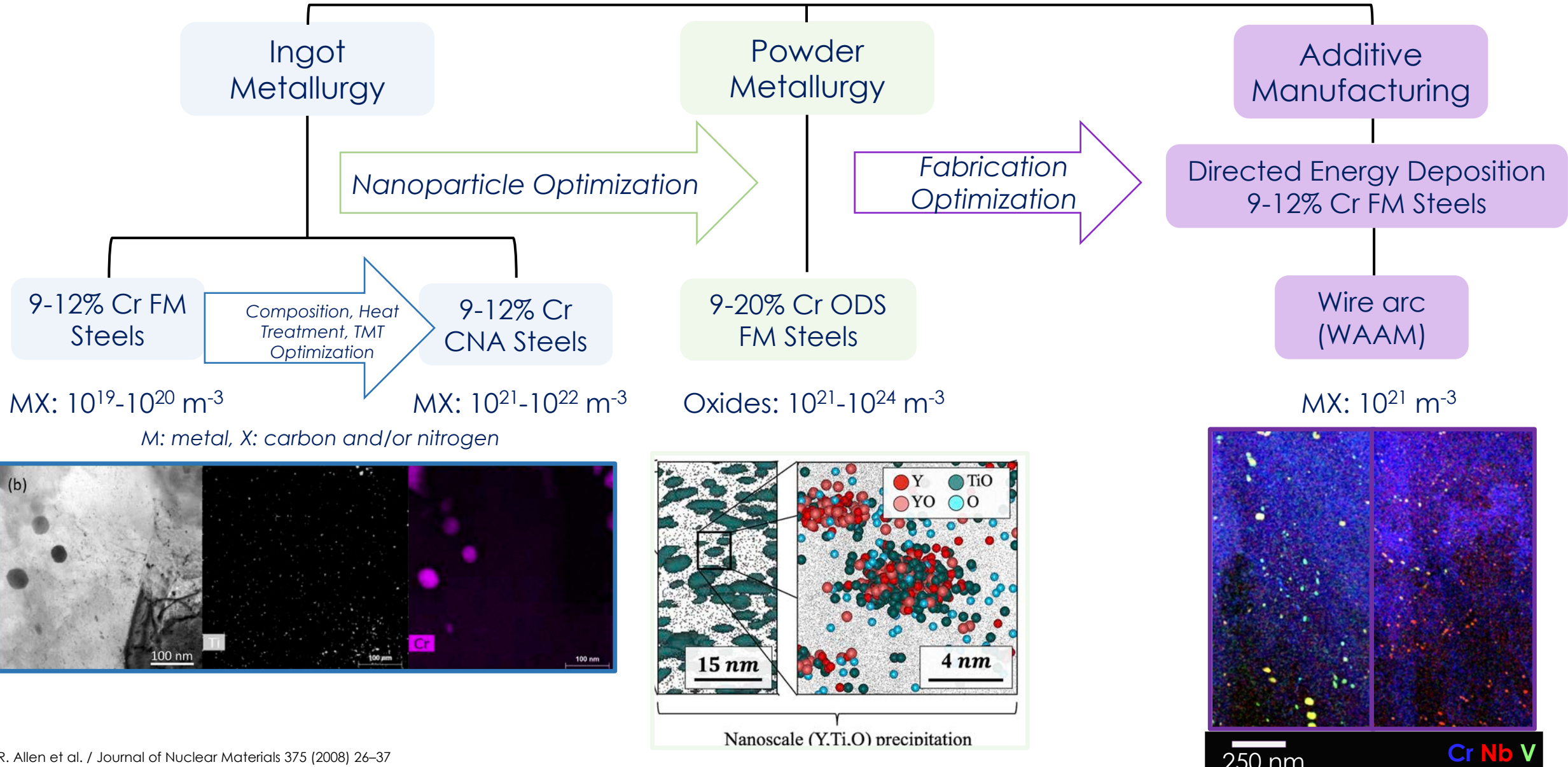
Resist radiation embrittlement

Creep resistance

Resist void swelling

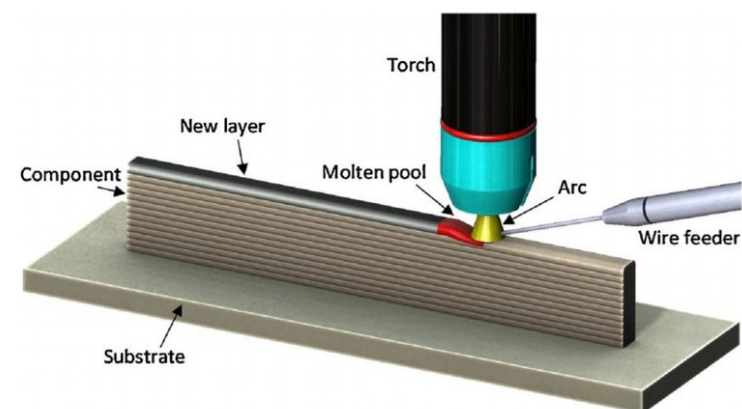
High strength & good ductility

9-20% Cr Alloy Development for Nuclear Reactor Core Internal and External Components



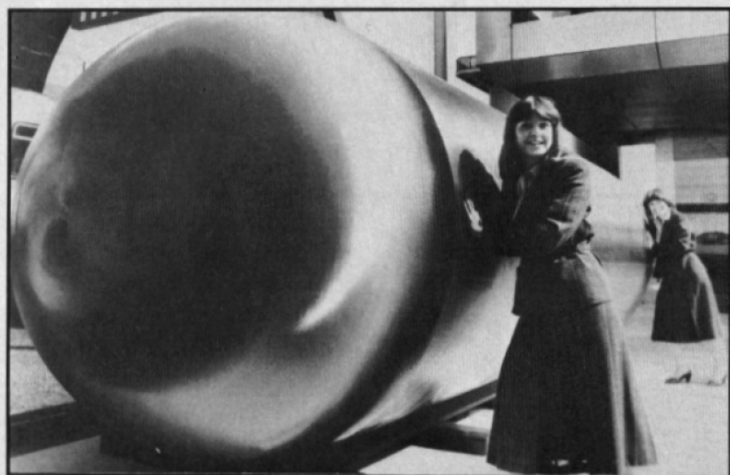
WAAM is preferred technique for RPV Fabrication

Wire arc AM process

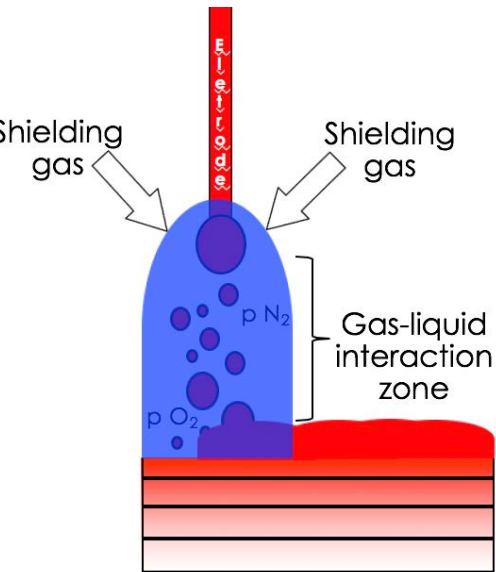


High deposition rates achievable

Fabricate large, non-complex geometries



Tailor structure of materials via control of processing parameters



A shielding gas is often used in order to control the arc stability, inclusion content, and microstructure in steel welds.

This experiment aims to:

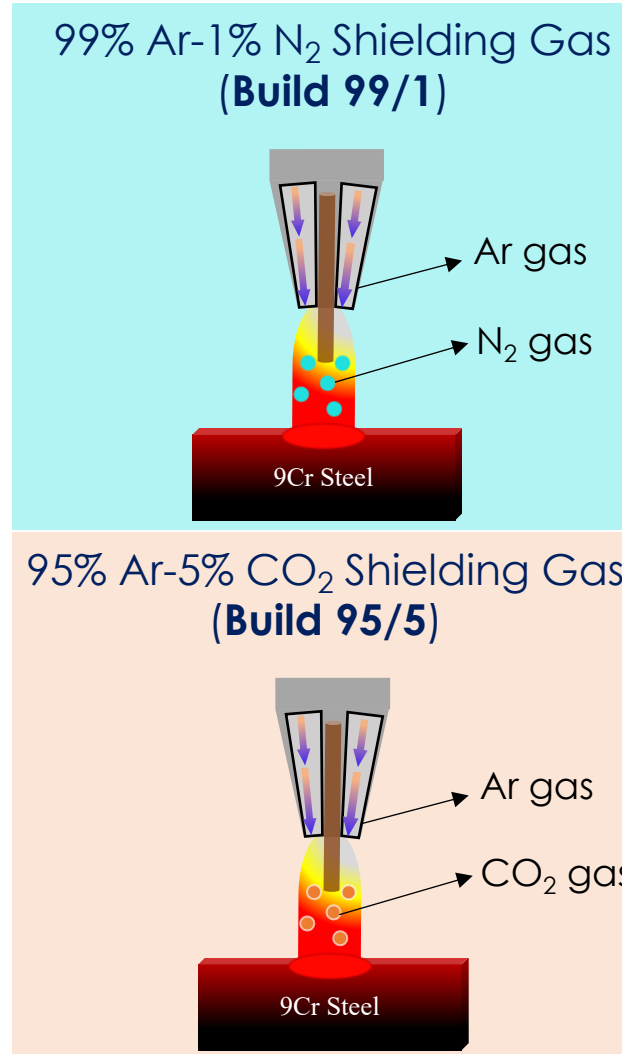
Assess WAAM for FM fabrication

Mimic or improve upon wrought properties

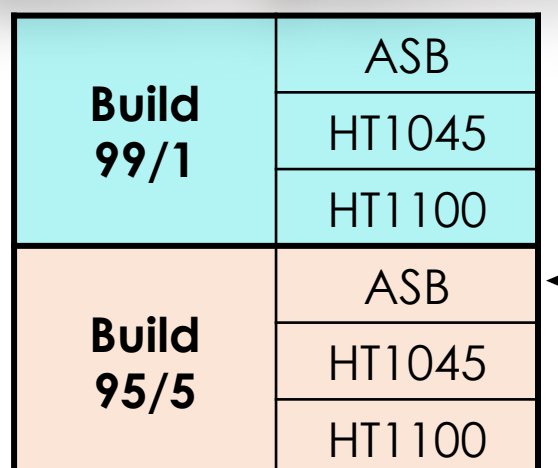
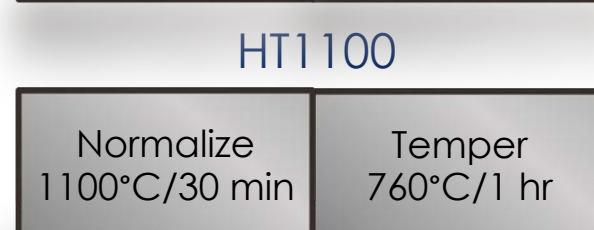
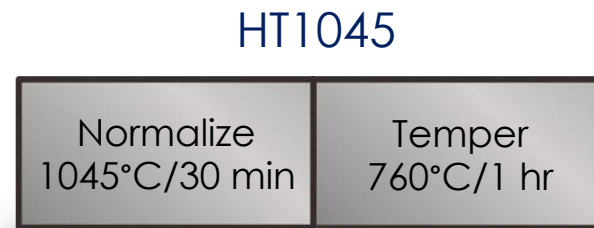
Control precipitate structure with AM processing parameters

Objective: Engineer MX precipitate morphology and size distribution in Grade 91 by altering the N₂ composition in the shielding gas used during additive manufacturing

1. Build

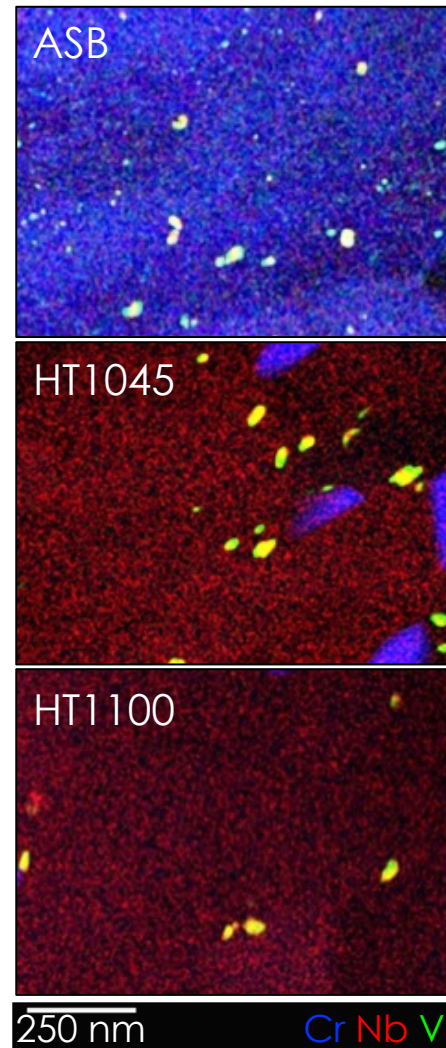


2. Heat Treat



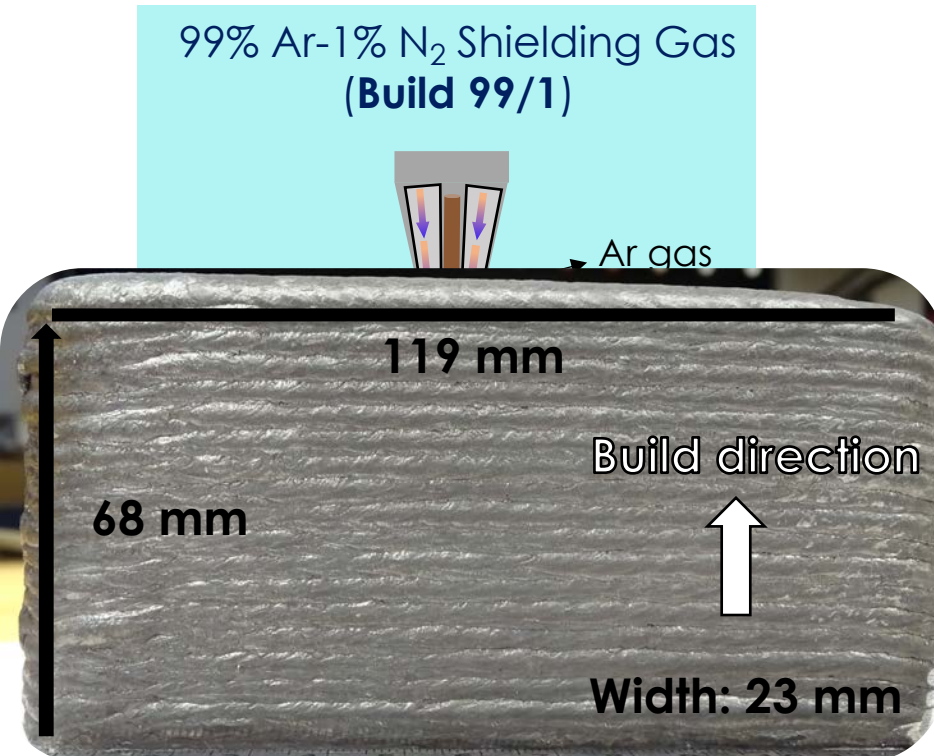
ASB=As-Built
(non-heat-treated)

3. Characterize

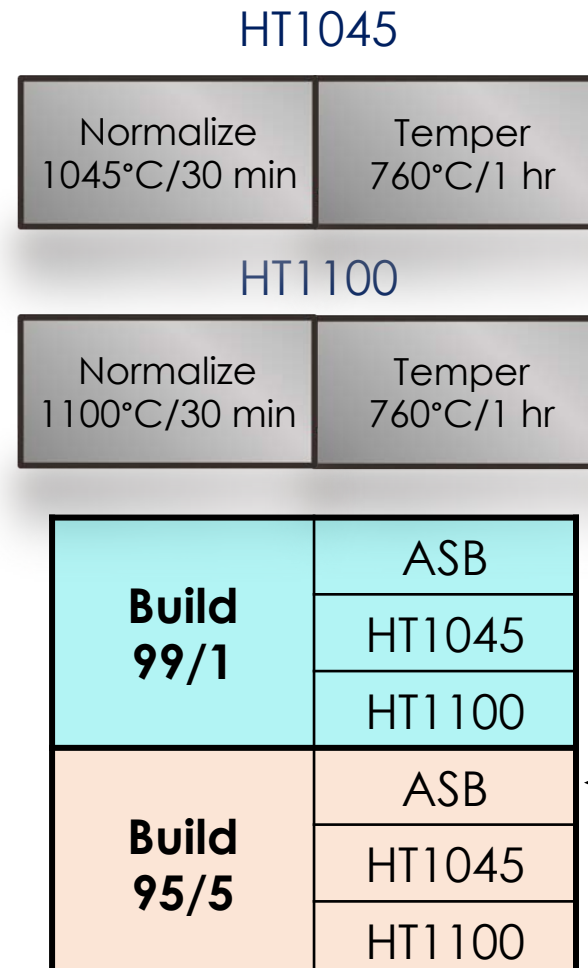


Objective: Engineer precipitate morphology and size distribution in Grade 91 by altering shielding gas composition during additive manufacturing

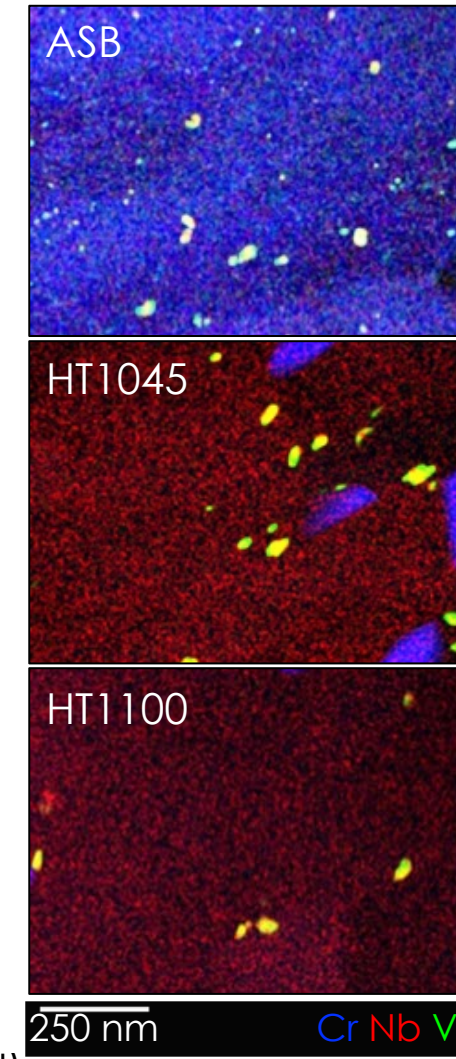
1. Build



2. Heat Treat

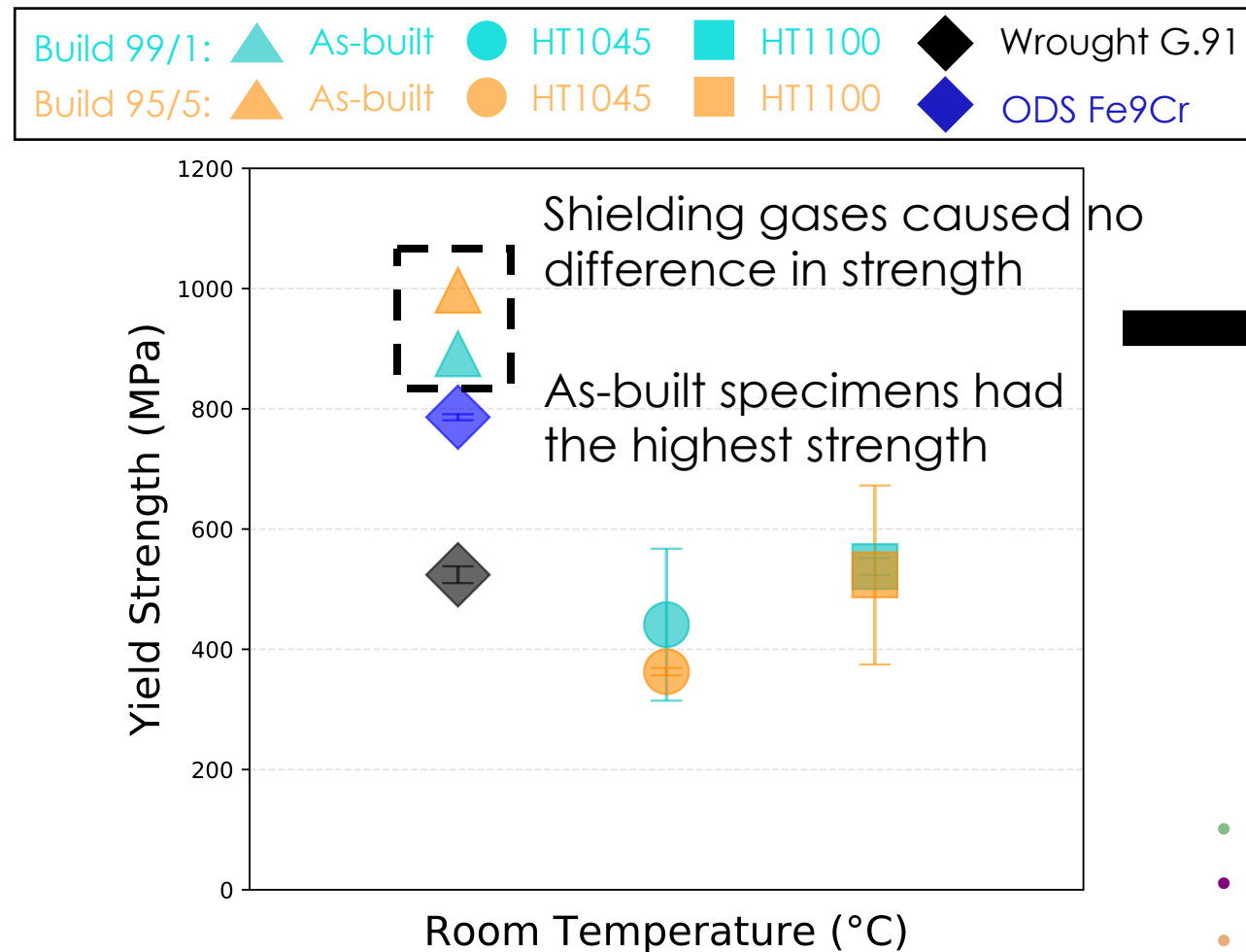


3. Characterize

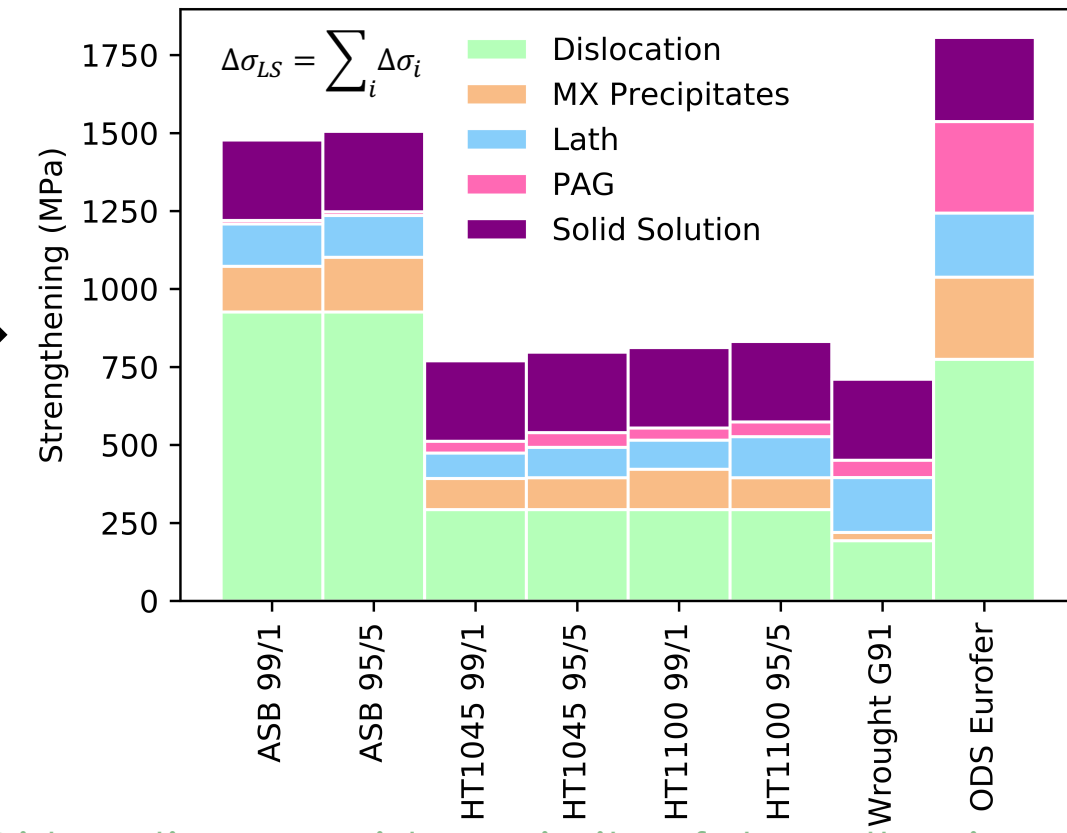


Mechanical Properties

Room Temperature Yield Strength



Strengthening Contributions

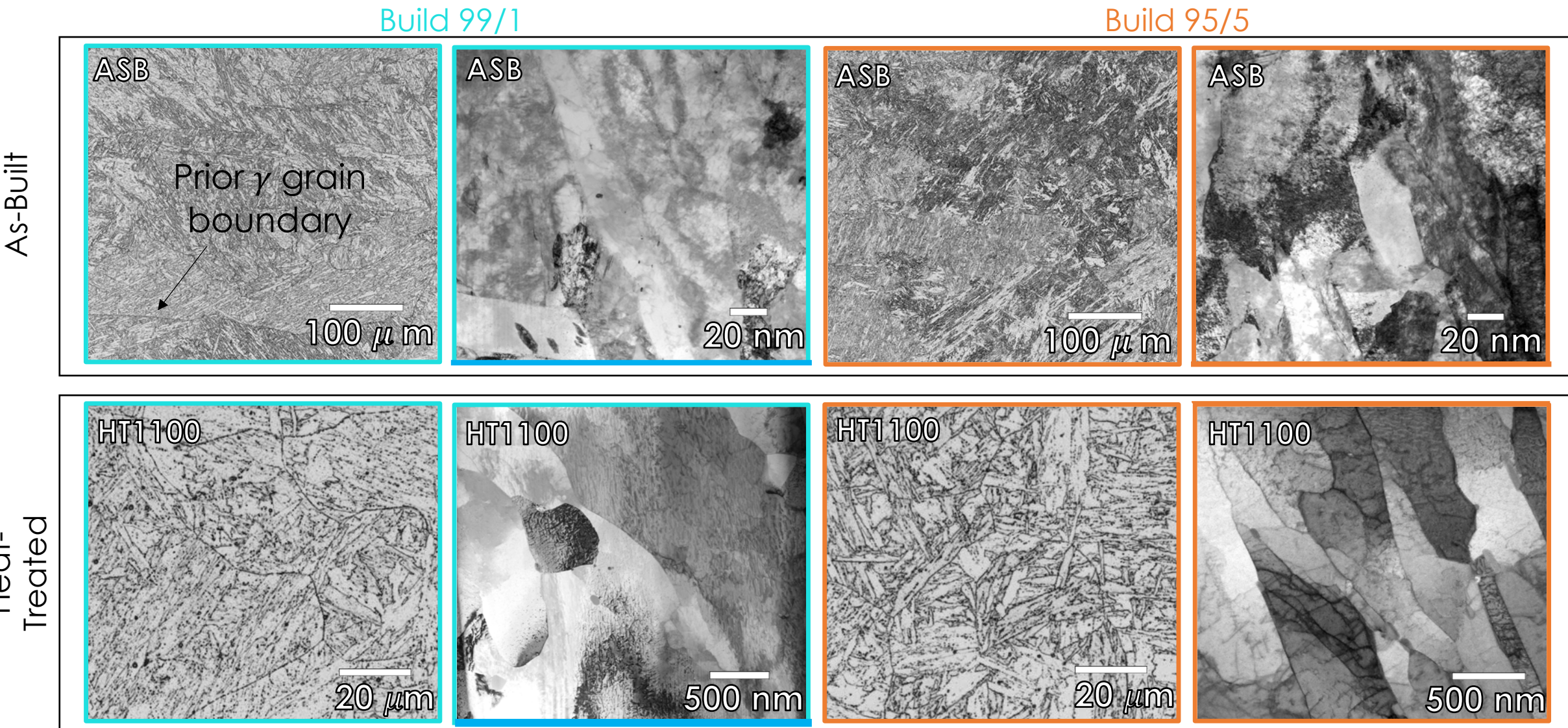


- Dislocations provide majority of strengthening
- Solid solution strengthening does not change
- The as-printed WAAM specimens had greater precipitation strengthening factors than the heat-treated WAAM specimens by ~20-75 MPa and than the wrought Grade 91 specimens by ~120-145 MPa⁶

	Build 99/1			Build 95/5			Wrought Grade 91		ODS Fe 9Cr
	ASB	HT1045	HT1100	ASB	HT1045	HT1100			
USE (J)	-	31.6 J	30.1 J	-	25.4 J	26.3 J	24.2*	23*	45 J
DBTT (°C)	>RT	-67°C	-49°C	>RT	-65°C	-62°C	-64°C	-17°C	-60°C

General Microstructure

Representative of wrought FM steels: laths, packets, and prior austenite grain boundaries



Shielding Gas Effect on Composition

	Oxygen Content (wt. %)	Carbon Content (wt. %)	Nitrogen Content (wt. %)
Wire Metal	0.008	0.08	0.04
Build 99/1	0.0178	0.072	0.0648
Build 95/5	0.0316	0.093	0.0386

Build 99/1: 62% increase in N

Build 95/5: 16.25%
increase in C

How do these changes compare to values from literature?

Shielding Gas Effect on Composition

	Oxygen Content (wt. %)	Carbon Content (wt. %)	Nitrogen Content (wt. %)
Wire Metal	0.008	0.08	0.04
Build 99/1	0.0178	0.072	0.0648
Build 95/5	0.0316	0.093	0.0386

Build 99/1: 62% increase in N

Build 95/5: 16.25%
increase in C

ASME Code for Wrought Grade 91

C
0.06-0.15 wt.%
N
0.025-0.08 wt.%

Welded Grade 91

SAW: no shielding gas

18% decrease in C

34% decrease in N

GTAW: 99.7% Ar

27% decrease in C

GTAW: 95% Ar+5% CO₂

38% increase in C

GTAW: 100% Ar

63% increase in C

GTAW: 100% CO₂

38% increase in C

Welded Fe

Auto-GTA: 95% Ar+5% N₂

1,800% increase in N

Auto-GTA: 80% Ar+20% N₂

2,900% increase in N

No consistent trends seen in C or N uptake, but uptake depends on base metal, filler metal, and shielding gas composition

ASB specimens contain C and N contents within the ranges designated by ASME

Additions of 5% CO₂ and 1% N₂ to the Ar shielding gases affected the final the C and N compositions

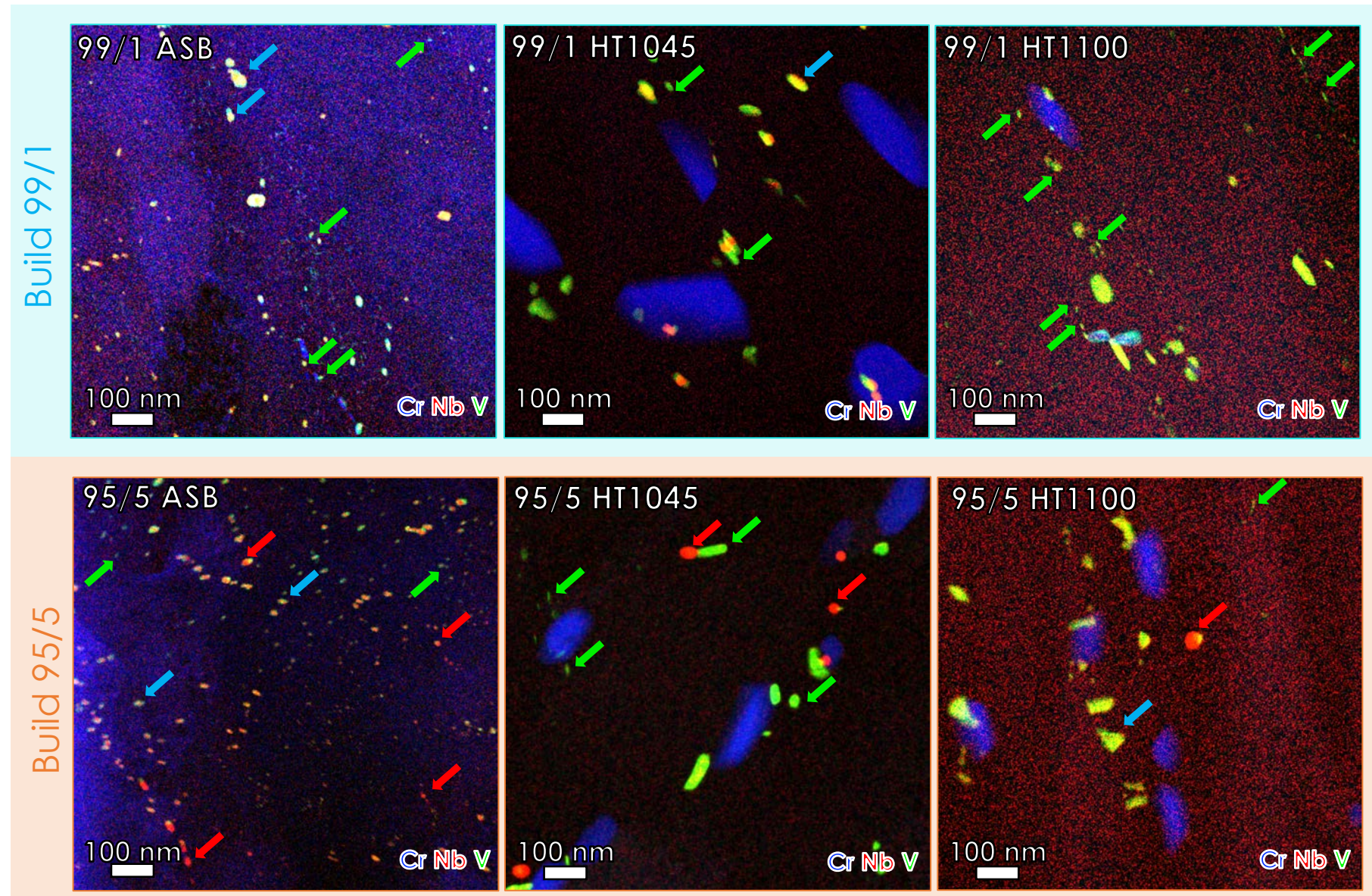
Shielding Gas Effect on MX Precipitation

Three small MX-type precipitates formed in the AM materials.

Red arrows:
Type I-Nb(C,N)

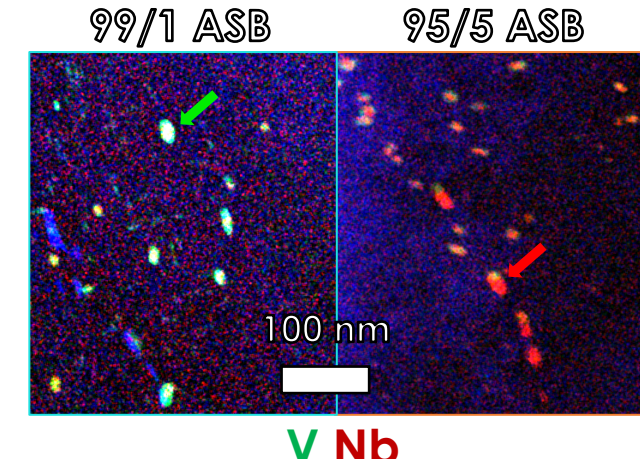
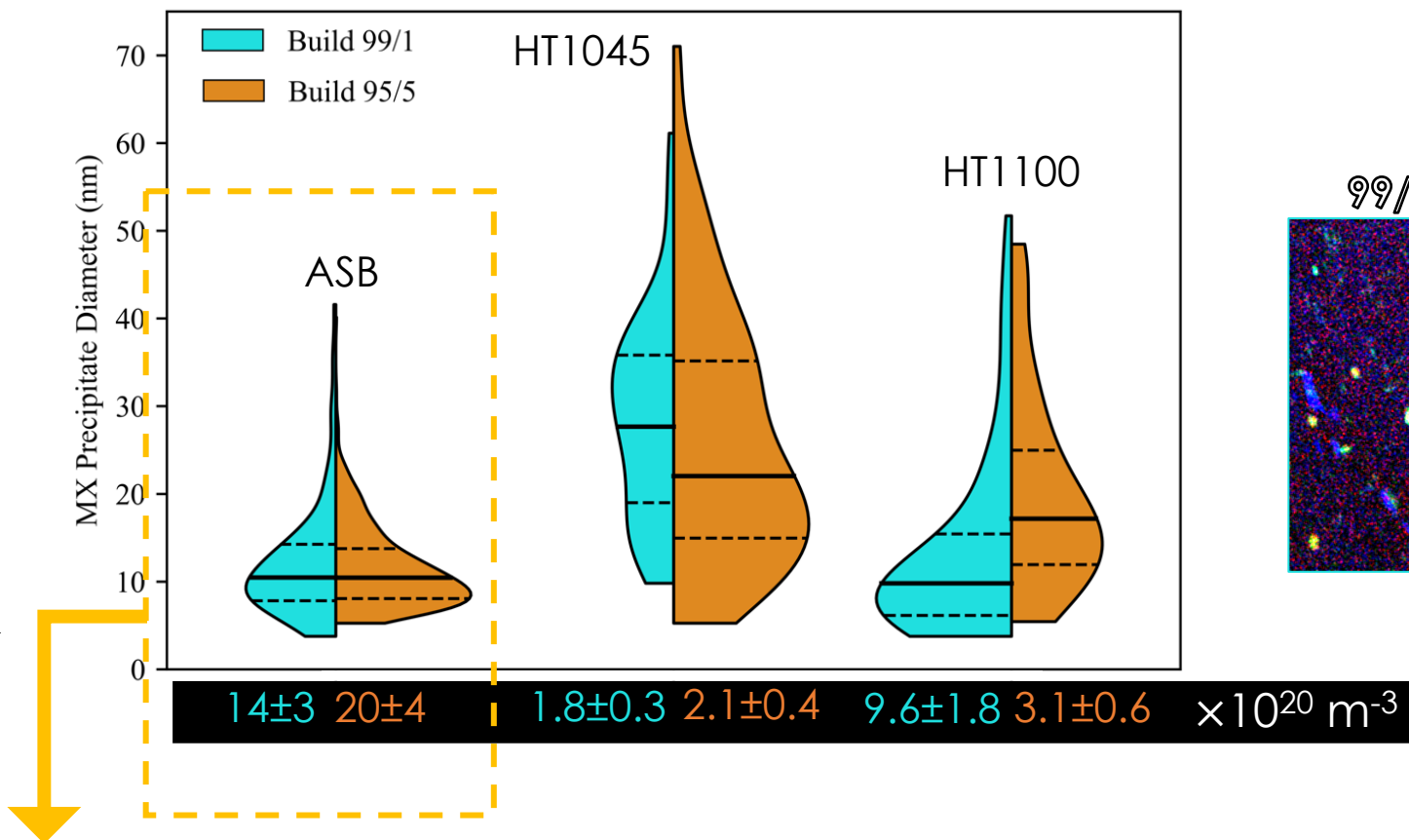
Green arrows:
Type II-VN
Type III-VN

Blue arrows:
Type II-(Nb,V)(C,N)



Shielding Gas Effect on MX Precipitation

Small precipitates are preferred.



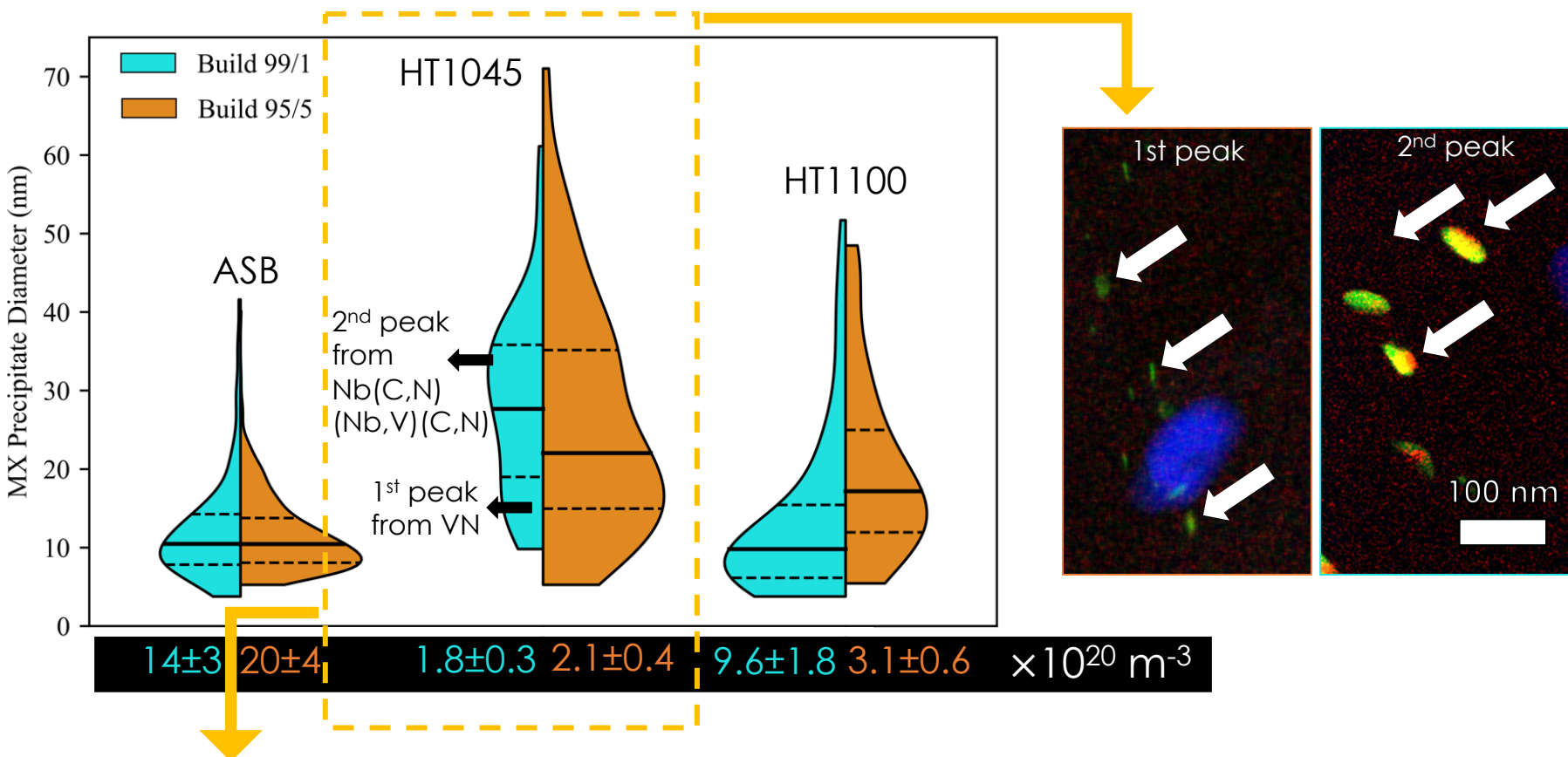
ASB specimens exhibit very fine, left-skewed size distributions

- N₂ additions to the shielding gas did not significantly affect shape of size distribution
- N₂ gas most greatly affected the **composition** and **morphology** of the MX precipitates by driving VN precipitation

ASB 99/1 has 3.8x more Type II-VN than ASB 95/5

ASB 95/5 has 2.3x more Type II-(Nb,V)(C,N) than ASB 99/1

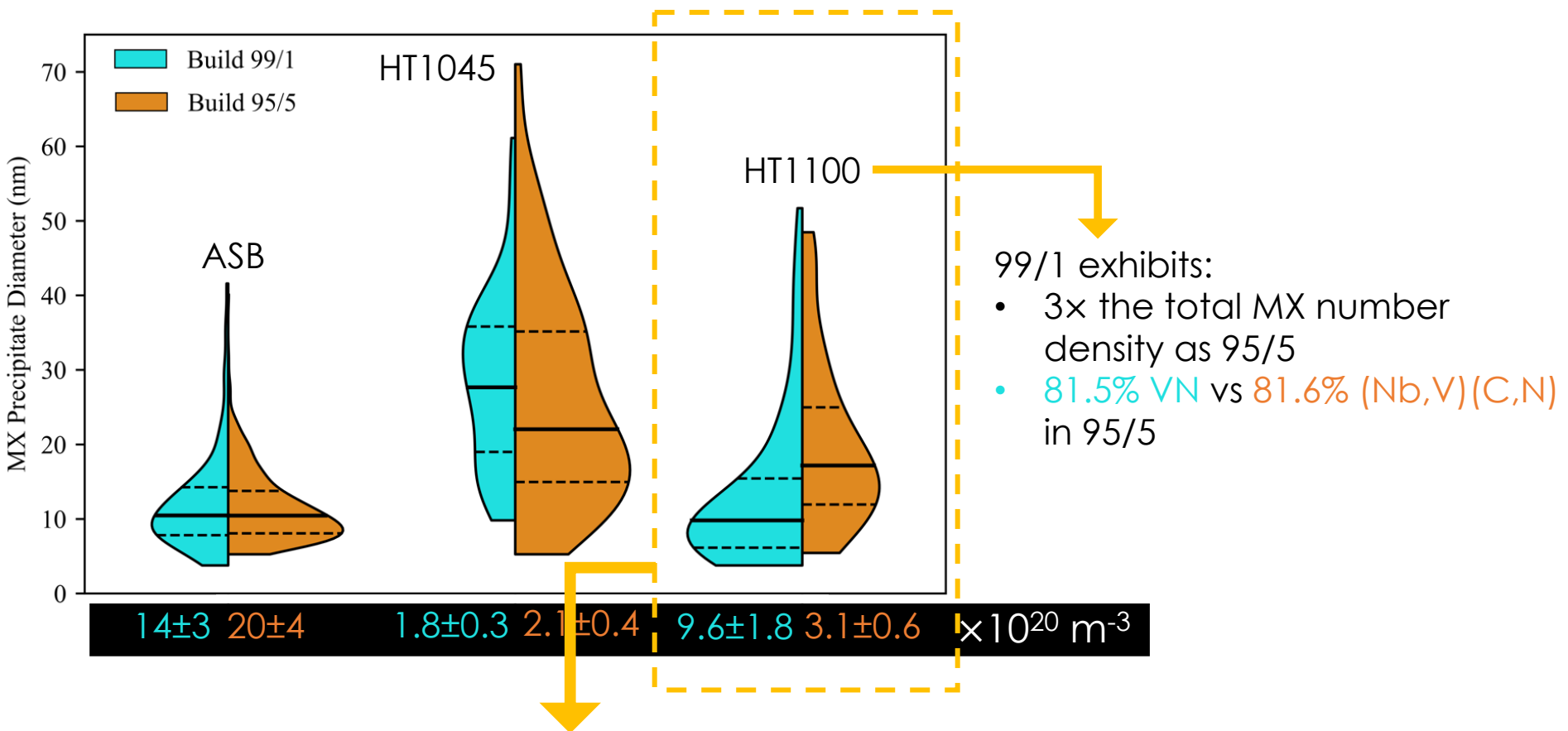
Shielding Gas Effect on MX Precipitation



HT1045 specimens exhibit bimodal size distributions

- This suggests that the MX precipitates were not fully dissolved during austenitization
 - Nb-containing Type-I and Type-II precipitates appeared to agglomerate and coarsen
 - Many V-rich precipitates dissolved and reprecipitated

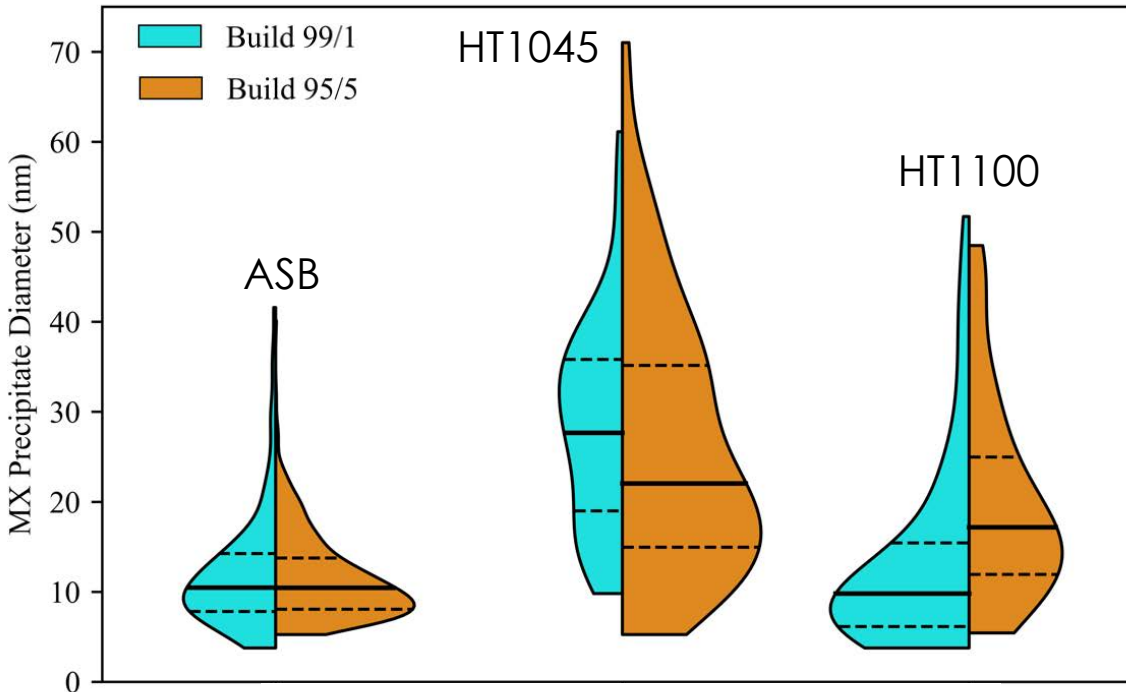
Shielding Gas Effect on MX Precipitation



HT1100 specimens exhibit fine, left-skewed size distributions similar to ASB but elongated

- This shape suggests that MX precipitates were almost fully dissolved at the higher austenitization temperature of 1100°C
- Higher N content of 99/1 caused increased MX precipitate density and smaller precipitate sizes

Shielding Gas Effect on MX Precipitation



WAAM:

- Controlled MX precipitate chemistry and temperature stability via shielding gas composition
- Increased MX precipitation over Wrought Grade 91 (10^{19} - 10^{20} m^{-3})

Shielding Gas Effect on Sink Strength

Sink strength is proportional to precipitate number density and precipitate size:

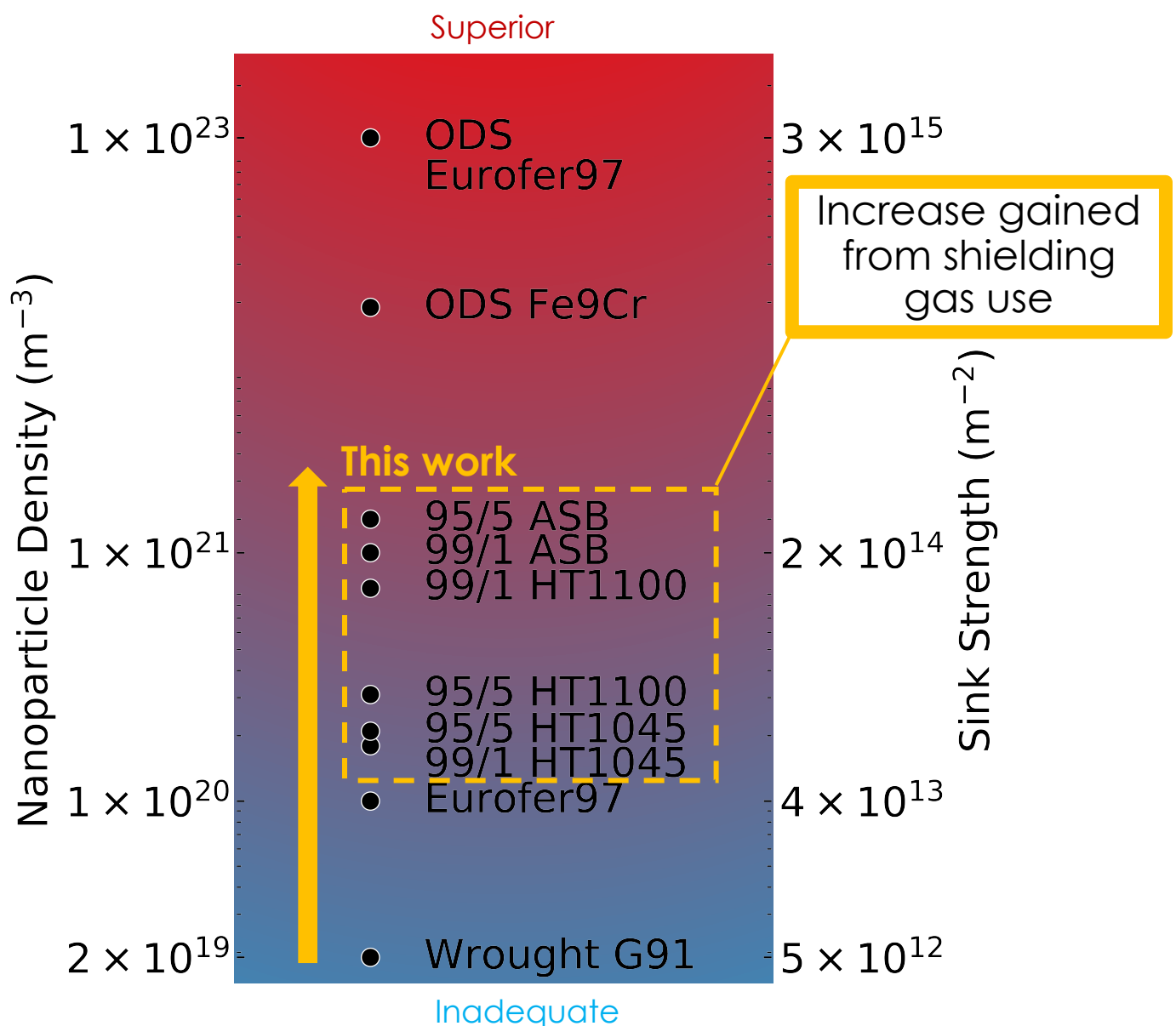
$$S_{j,ppt} = 4\pi r_{ppt} N_{ppt} Y_j$$

$$S_{total,ppt} = \sum_{j=i,v} S_{j,ppt}$$

$$Y_i = 1 + \frac{(Z_i - Z_v) \rho_d}{Z_v \rho_d + 4\pi r_{ns} N_{ns}}$$

$$Y_v = 1$$

Material		S_{MX} or S_{oxide} (m^{-2})	S_{MX}/ S_{oxide} Percent of Total	S_{Total} (m^{-2})
Build 99/1	ASB	2×10^{14}	5.8%	4×10^{15}
	HT1045	6×10^{13}	10.9%	6×10^{14}
	HT1100	2×10^{14}	20.9%	8×10^{14}
Build 95/5	ASB	3×10^{14}	9.3%	3×10^{15}
	HT1045	7×10^{13}	13.4%	5×10^{14}
	HT1100	8×10^{13}	9.1%	9×10^{14}
Wrought Grade 91		5×10^{12}	1.3%	4×10^{14}
Eurofer97		4×10^{13}	5.3%	7×10^{14}
ODS Eurofer97-1 ($N_{oxide} = 1 \times 10^{23} m^{-3}$)		5×10^{15}	55.4%	9×10^{15}
ODS Eurofer97-2 ($N_{oxide} = 1 \times 10^{22} m^{-3}$)		5×10^{14}	14.4%	4×10^{15}



Summary

Successfully fabricated FM steel Grade 91 with DED-AM technique

Improved upon wrought Grade 91 microstructure and mechanical properties

Proved ability to control MX precipitate chemistry and stability with shielding gas composition

Increased sink strength of Grade 91 using shielding gases that supersaturated C and N in the microstructure during AM

Conclusion

Small tweaks in the processing parameters during AM can produce vastly different microstructures, allowing for creative opportunities for hybrid materials processing



Paper to be submitted to
Acta Materialia this year



References

1. K. Sawada, F. Abe, et al, Data Sheets on the Elevated-Temperature Properties of 9Cr–1Mo–V–Nb Steel Tubes for Boilers and Heat Exchangers (ASME SA-213/SA-213M Grade T91), 9Cr–1Mo–V–Nb Steel Plates for Boilers and Pressure Vessels (ASME SA-387/SA-387M Grade 91) and 9Cr–1Mo–V–Nb Steel, NIMS Creep Data Sheet No. 43A Natl. Inst. Mater. Sci. DOI: 10.11 (2014).
2. E. Lucon, Mechanical properties of two improved eurofer ods steels before and after low dose neutron irradiation at 300 °C, Fusion Sci. Technol. 56 (2009) 289–294. <https://doi.org/10.13182/FST09-A8916>.
3. E. Lucon, Tensile and Fracture Toughness Properties of EUROFER ODS ("EU Batch" - 6 mm Plate) in the Unirradiated Condition, (2006).
4. E.I. Galindo-Nava, P.E.J. Rivera-Díaz-Del-Castillo, A model for the microstructure behaviour and strength evolution in lath martensite, Acta Mater. 98 (2015) 81–93. <https://doi.org/10.1016/j.actamat.2015.07.018>.
5. N. Sridharan, K. Field, A Road Map for the Advanced Manufacturing of Ferritic-Martensitic Steels, Fusion Sci. Technol. 75 (2019) 264–274. <https://doi.org/10.1080/15361055.2019.1577124>.
6. R.L. Klueh, D.R. Harries, High-Chromium Ferritic and Martensitic Steels for Nuclear Applications, 2001. <https://doi.org/10.1520/MONO3-EB>.
7. R.L. Klueh, Elevated-Temperature Ferritic and Martensitic Steels and Their Application To Future, 2004.
8. J. Fu, J.C. Brouwer, R.W.A. Hendrikx, I.M. Richardson, M.J.M. Hermans, Microstructure characterisation and mechanical properties of ODS Eurofer steel subject to designed heat treatments, Mater. Sci. Eng. A. 770 (2020). <https://doi.org/10.1016/j.msea.2019.138568>.
9. A. Das, P. Chekhonin, E. Altstadt, F. Bergner, C. Heintze, R. Lindau, Microstructural characterization of inhomogeneity in 9Cr ODS EUROFER steel, J. Nucl. Mater. 533 (2020) 152083. <https://doi.org/10.1016/j.jnucmat.2020.152083>.
10. L. Tan, L.L. Snead, Y. Katoh, Development of new generation reduced activation ferritic-martensitic steels for advanced fusion reactors, J. Nucl. Mater. 478 (2016) 42–49. <https://doi.org/10.1016/j.jnucmat.2016.05.037>.
11. C. Heintze, F. Bergner, A. Ulbricht, M. Hernández-Mayoral, U. Keiderling, R. Lindau, T. Weissgärber, Microstructure of oxide dispersion strengthened Eurofer and iron-chromium alloys investigated by means of small-angle neutron scattering and transmission electron microscopy, J. Nucl. Mater. 416 (2011) 35–39. <https://doi.org/10.1016/j.jnucmat.2010.11.102>.
12. L.K. Mansur, Theory and experimental background on dimensional changes in irradiated alloys *, 216 (2008) 97–123.
13. A.D. Brailsford, L.K. Mansur, The Effect of Precipitate-Matrix Interface Sinks on the Growth of Voids in the Matrix, J. Nucl. Mater. 103 & 104 (1981) 1403–1408.
14. A.D. Brailsford, R. Bullough, The Rate Theory of Swelling in Irradiated Metals, J. Nucl. Mater. 44 (1972) 121–135.
15. A.D. Brailsford, R. Bullough, The Theory of Sink Strengths, 302 (1981) 87–137.
16. Shuai Xu et al., Mechanical properties evaluation and plastic instabilities of Fe-9%Cr ODS T steels, Fusion Engineering and Design 149 (2019) 111335

MECHANICAL PROPERTIES: Ref. 1-10

SINK STRENGTH: Ref. 6-15

Extra Slides

Parameter	ASB		HT1045		HT1100	
Build	99/1	95/5	99/1	95/5	99/1	95/5
Mean Size (nm)	12±7	12±5	28±11	26±15	13±11	20±11
Number Density ($\times 10^{20} \text{ m}^{-3}$)	14±3	20±4	1.8±0.3	2.1±0.4	9.6±1.8	3.1±0.6
Vol. Fract.	0.016± 0.003	0.015±0.005	0.022± 0.004	0.022± 0.005	0.025± 0.005	0.016± 0.009
Located on Grain Boundaries	20%	14%	25%	47%	44%	50%
Type-I Nb(C,N)	0%	5.7%	0%	26.3%	0%	2.6%
Type-II VN	51.5%	9.6%	10%	15.8%	81.5%	13.2%
Type-II (Nb,V)(C,N)	48.5%	79.6%	90%	47.4%	18.5%	81.6%
Type-III VN wings	0%	5.1%	0%	10.5%	0%	2.6%

Extra Slides

		S_d (m ⁻²)	S_d Percent of Total	S_{GB} (m ⁻²)	S_{GB} Percent of Total	S_{MX} or S_{oxide} (m ⁻²)	S_{MX}/ S_{oxide} Percent of Total	S_{M23C6} (m ⁻²)	S_{M23C6} Percent of Total	S_{Total} (m ⁻²)
Build 99/1	ASB	2×10^{15}	54.4%	1×10^{15}	39.8%	2×10^{14}	5.8%	3×10^{12}	0.1%	4×10^{15}
	HT1045	2×10^{14}	34.6%	3×10^{14}	51.2%	6×10^{13}	10.9%	2×10^{13}	3.3%	6×10^{14}
	HT1100	2×10^{14}	25.8%	4×10^{14}	51.6%	2×10^{14}	20.9%	1×10^{13}	1.7%	8×10^{14}
Build 95/5	ASB	2×10^{15}	63.9%	8×10^{14}	26.8%	3×10^{14}	9.3%	-	0.0%	3×10^{15}
	HT1045	2×10^{14}	38.1%	2×10^{14}	44.3%	7×10^{13}	13.4%	2×10^{13}	4.3%	5×10^{14}
	HT1100	2×10^{14}	22.9%	6×10^{14}	63.6%	8×10^{13}	9.1%	4×10^{13}	4.5%	9×10^{14}
Wrought Grade 91		1×10^{14}	25.7%	3×10^{14}	70.5%	5×10^{12}	1.3%	9×10^{12}	2.4%	4×10^{14}
Eurofer97		2×10^{14}	27.9%	5×10^{14}	65.9%	4×10^{13}	5.3%	7×10^{12}	1.0%	7×10^{14}
ODS Eurofer97-1 ($N_{oxide} = 1 \times 10^{23} m^{-3}$) [10–13]		1×10^{15}	15.4%	3×10^{15}	29.2%	5×10^{15}	55.4%	5×10^{11}	0.0%	9×10^{15}
ODS Eurofer97-2 ($N_{oxide} = 1 \times 10^{22} m^{-3}$) [10–13]		1×10^{15}	40.0%	2×10^{15}	45.6%	5×10^{14}	14.4%	5×10^{11}	0.0%	4×10^{15}